





Investigation of acousto-optic interaction with momentum mismatching considering acoustic anisotropy in birefringent crystal

GUOFENG ZHENG,¹  ZHICHAO LV,¹  CHUNGUANG ZHANG,^{1,2,3}
YIZHE ZHANG,¹ JIAKANG LI,¹ SHUFAN YANG,^{2,4}
AND HAO WANG^{1,2,5}

¹Key Laboratory of Optoelectronic Science and Technology for Medicine, Fujian Provincial Key Laboratory of Photonics Technology, Fujian Provincial Engineering Technology Research Center of Photoelectric Sensing Application, College of Photonic and Electronic Engineering, Ministry of Education, Fujian Normal University, Fujian 350007, China

²School of Computing, Engineering & the Built Environment, Edinburgh Napier University, Edinburgh, Scotland, EH10 5DT, UK

³cgzhang@fjnu.edu.cn

⁴S.Yang@napier.ac.uk

⁵haowang@fjnu.edu.cn

Abstract: In this work, the momentum mismatching based on which the acousto-optic (AO) transfer function and diffraction efficiency was acquired, was calculated considering the properties of AO crystals in AO interactions in acousto-optic tunable filter (AOTF). Transfer functions were obtained using a 4f optical system combined with AOTF and compared with theoretical calculations. It demonstrated the influence of acoustic energy shift on the AO interaction which should be considered in the design of AOTF.

© 2024 Optica Publishing Group under the terms of the [Optica Open Access Publishing Agreement](#)

1. Introduction

AO techniques are currently widely applied across various domains of science and engineering such as spectroscopy, optical imaging, and etc [1–4]. Spectral imaging capable of simultaneously acquiring the image and spectral information of target has becoming one of the frontiers of optics [5,6]. Non-collinear AOTF is a typical AO device designed based on the principle of abnormal Bragg diffraction with the advantages such as compact size, rapid tuning and high diffraction efficiency and it could provide a good light-dividing technique for spectral imaging [7–9]. Typically, the AO interaction is analyzed using the plane wave approximation, wherein the acoustic wave is considered as a single plane wave propagating perpendicular to the transducer [10]. The frequency and angular dependence of AO interactions are determined through the analysis of momentum mismatching caused by variations in the directions of the acoustic and incident light waves considering dispersion which was important not only in AO interaction but also in sensing [11]. This analytical approach is commonly known as the momentum mismatching method [12].

The accurate calculation of momentum mismatching is important in the study of AO procedure. I. C. Chang et al. demonstrated that the direction of momentum mismatching should be perpendicular to the boundary of the AO medium, i.e., along the [001] axis within the (1 $\bar{1}$ 0) plane of AO crystal [13,14]. While V. B. Voloshinov and his colleagues proposed an alternative perspective, suggesting that the momentum mismatching should orient perpendicular to the boundary of the acoustic column propagating in the crystal for the acoustic energy deviation due to the strong acoustic anisotropy of the crystal should be considered [15,16]. However, up to now, a definitive and universally accepted method for describing the AO process has not been

conclusively established. Therefore, we conducted a detailed analysis on these two methods in theory and made further discussions and comparisons with experiments.

In this paper, an AOTF based spatial filtering system was designed, measured transfer functions were then compared with the theoretical results calculated based on the methods mentioned above. It was demonstrated that the acoustic anisotropy in the AO interaction procedure should be considered, because it not only altered the structure of the acoustic beam but also introduced the shifts of acoustic energy and even affected the AO interaction [17,18].

2. Theoretical analysis of momentum mismatching

Figure 1 demonstrates the vector diagram of AO interactions in a non-collinear AOTF. Here k_i , k_d , K , Δk , θ_i , θ_d , θ_a , n_o , n_e and λ are the wave vector of the incident e-polarized light, the wave vector of diffracted o-polarized light, the acoustic wave vector, the momentum mismatching (undefined direction), the polar angle of the incident light, the polar angle of the diffracted light, the acoustic polar angle, the refractive index of the o-polarized light, the refractive index of the e-polarized light and the wavelength, respectively.

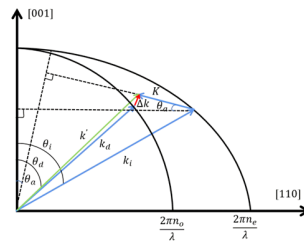


Fig. 1. Non-collinear AO interaction vector diagram.

In AO interaction $k_i + K = k' = k_d + \Delta k$, here, $\Delta k = 0$ means the momentum matching and $k_i + K = k_d$ [12]. The formulas for calculating the wave vectors are as follows:

$$k_i = \frac{2\pi n_i}{\lambda}, k_d = \frac{2\pi n_d}{\lambda}, K = \frac{2\pi f_a}{V} \quad (1)$$

where f_a , V , n_i and n_d are the ultrasonic frequency, the ultrasonic speed, the refractive index of the incident light and the refractive index of the diffracted light, respectively. Here n_i and n_d could be expressed as:

$$n_i = \left(\frac{\cos^2 \theta_i}{n_o^2} + \frac{\sin^2 \theta_i}{n_e^2} \right)^{-\frac{1}{2}}, n_d = n_o \quad (2)$$

And the frequency tuning relation could be derived as follows:

$$f_a = \left(\frac{V}{\lambda} \right) [n_i^2 + n_d^2 - 2n_i n_d \cos(\theta_i - \theta_d)]^{\frac{1}{2}} \quad (3)$$

$$f_a = \left(\frac{V}{\lambda} \right) \left[n_i \sin(\theta_i - \theta_a) - \sqrt{n_o^2 - n_i^2 \cos^2(\theta_i - \theta_a)} \right] \quad (4)$$

These two equations are equivalent under the condition of momentum matching [15].

The diffraction efficiency in AO interaction could be expressed as [12]:

$$\eta = (\xi^2) \frac{\sin^2 \delta}{\delta^2} \quad (5)$$

Here, $\delta^2 = \zeta^2 + \xi^2$, $\zeta = \Delta k L$, $\xi^2 = \xi_0 \xi_1 / 4$, $\xi_0 = -2\pi \Delta n_0 L / \lambda$, $\xi_1 = -2\pi \Delta n_1 L / \lambda$. L is the AO interaction length. Δn_0 and Δn_1 are the refractive index changes. ξ is typically set to π and the incident light is diffracted into the first-order of Bragg diffraction with 100% efficiency.

In order to calculate the diffraction efficiency which is a key of AO interaction, the momentum mismatching should be determined and calculated at first. Figure 2 demonstrates the vector diagram of AO interaction when the momentum mismatching is oriented along [001] or in the direction perpendicular to the acoustic energy. Here, the coincideration of [001] and optical axis of AO crystal will facilitate the analysis and calculation of momentum mismatching, if [001] is not on the optical axis, the relationship between the momentum mismatching and acoustic angle and etc. keeps unchanged.

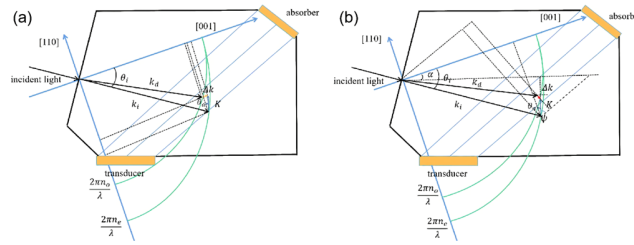


Fig. 2. Vector diagrams of AO interaction (a) Δk_1 along the [001] axis; (b) Δk_2 along the direction perpendicular to the acoustic energy propagation.

Based on the geometric relationship shown in Fig. 2, we can calculate the momentum mismatching, denoted as Δk_1 and Δk_2 respectively, as demonstrated below:

$$\Delta k_1 = k_i \cos \theta_i + K \sin \theta_a - \sqrt{k_o^2 - (k_i \sin \theta_i - K \cos \theta_a)^2} \quad (6)$$

$$\Delta k_2 = k_i \cos[\psi - (\theta_i - \theta_a)] - K \sin \psi - \sqrt{k_o^2 - (k_i \sin[\psi - (\theta_i - \theta_a)] + K \cos \psi)^2} \quad (7)$$

Here, ψ represents the shift angle of acoustic energy, expressed as $\psi = \tan^{-1} \frac{V_z^2 - V_t^2}{2V^2} \sin 2\theta_a$, where V_z is the phase velocity value along the [001] axis and $V_z = 2104\text{m/s}$, V_t is the phase velocity value along the [110] axis and $V_t = 616\text{m/s}$, V is the speed of sound in an arbitrary direction on the (11(-)0) plane, given by: $V = \sqrt{V_t^2 \cos^2 \theta_a + V_z^2 \sin^2 \theta_a}$ [12].

As known, the diffraction efficiency of AOTF is closely related to the momentum mismatching. And the transfer function can be derived from the diffraction efficiency [19]. For any noncollinear AOTF, the transfer function enables bandpass filtering of spatial frequencies, with applications in contrast-enhanced imaging and the visualization of phase objects [20,21]. Therefore, the diffraction efficiencies of AOTF based on Δk_1 and Δk_2 are calculated as functions of the incident deviation angle, respectively, as shown in Fig. 3.

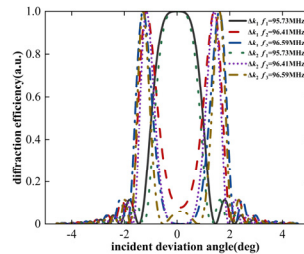


Fig. 3. Calculated diffraction efficiency of AOTF based on Δk_1 and Δk_2 , respectively.

Here the parameters are selected as: $\lambda = 0.5328 \mu\text{m}$, $\theta_a = 6.8^\circ$, $\psi = 47.96^\circ$, $n_o = 2.30$, $n_e = 2.46$, $V = 660.45 \text{ m/s}$. And the corresponding frequency of sound wave and the optimal

incident angle are 95.73 MHz and 15.73° , respectively, calculated from Eq. (4) under momentum matching, where $df_a/d\theta_i = 0$. The incidence deviation angle in Fig. 3 is distributed on both sides relative to the optimal incidence angle, i.e., the optimum incidence angle corresponds to the position where the incidence offset angle is 0.

From Fig. 3 we can find that the calculated diffraction efficiencies with Δk_1 and Δk_2 have obvious differences. When $f_1 = 95.73$ MHz, the calculated full width at half maximum (FWHM) of diffraction efficiency based on Δk_2 is narrower than that calculated based on Δk_1 and the calculated diffraction efficiency based on Δk_2 decreases more quickly than that calculated based on Δk_1 which means the transfer function calculated based on Δk_2 is more sensitive to the incident deviation angle than that calculate based on Δk_1 , the sensitivity is crucial in contrast-enhanced imaging [22]. Regarding the evolution pattern of diffraction efficiency with the frequency of the sound, especially, the observed frequency differences (FD) which lead to the diffraction efficiency changing from maximal to minimum are 0.86 and 0.68 MHz, respectively, calculated using Δk_1 and Δk_2 . The discrepancy of 0.18 MHz in sound frequency will cause the wavelength difference that is too large to ignore, especially in the field of spectral analysis, where differences are usually on the scale of several nanometers in the visible range according to the tuning relation. Therefore, the selection of method for accurately calculating the momentum mismatching is of paramount importance.

3. Experimental results and discussion

To evaluate the methods on the calculation of momentum mismatching and select the proper one, we designed an experimental setup, shown in Fig. 4, and measured the transfer functions of the filtering process. This allowed us to capture the impact of momentum mismatching.

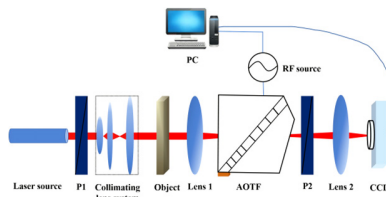


Fig. 4. Experimental setup.

In Fig. 4, the 4f optical system was used for AO spatial filtering. In the experiment, the laser light passing through polarizer P1, collimating lens system was focused into AOTF by lens 1. The AOTF, acting as a spatial filter, was placed on the rear focal plane of lens 1. The diffracted light passed through polarizer P2, which has an orthogonal polarization direction to P1, and was then imaged on CCD by lens 2. The RF source and CCD were controlled by a PC.

During experiment, when the wavelength of the incident light, which was 532.8 nm in this case, was selected, tuning RF, we could observe the spatial distribution of AO Bragg diffraction, shown in Fig. 5 (a), which was referred to as the visualization of two-dimensional spatial transfer function of the AOTF. Usually transfer function demonstrated the pattern of concentric rings with dark or bright spot corresponding to the change of AO diffraction efficiency.

Controlling RF, the darkest spot (DS) corresponding to the minimum of diffraction efficiency and brightest spot (BS) corresponding to the maximum of diffraction efficiency could be observed in the center of the transfer function shown in Fig. 5 (b) and (c), respectively.

The FD between the patterns of transfer function of DS and BS was very important in the control of the filtering mode, especially when AOTF acted as a spatial filter in contrast-enhanced imaging procedures [20,21]. On one hand, AOTF demonstrated contrast-enhanced imaging performance when the DS condition was satisfied, indicating the depression of lower spatial

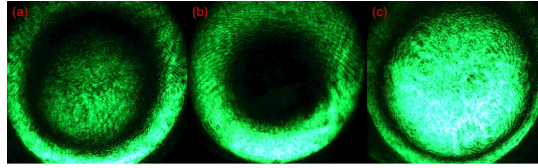


Fig. 5. Measured transfer functions of the AOTF:(a) transfer function of multi-ring patterns;(b) DS in diffraction;(c) BS in diffraction

frequency of the signal light. On the other hand, AOTF acted as a low pass filter when the BS condition was satisfied and the fine detail of image would be absent. Therefore, the accurate calculation of the transfer function, which was determined by precise momentum mismatch calculations, was crucial for the precise control of the spatial filtering mode of AOTF.

In AO interaction, shown in Fig. 1, momentum mismatching was mainly determined by the vectors of incident light and the propagating sound wave within the crystal. Here, we used FD to reflect changes in the transfer function due to momentum mismatching. Figure 6 demonstrated the relationship between FD and the incident wavelength while keeping the polar angle of the incident light and the sound wave vector unchanged. The spectral range was selected in 400-800 nm which was also the main spectral range for applications including optical sensors [23].

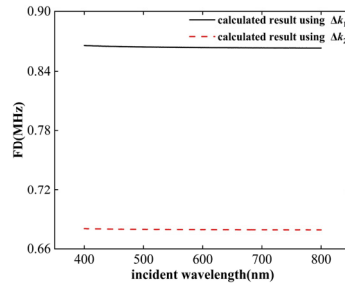


Fig. 6. Calculated relationship between FD and the wavelength of the incident light

From Fig. 6, it could be observed that FDs were not sensitive to the change of the wavelength of the incident light, despite the FDs calculated from Δk_1 and Δk_2 had distinct difference.

Figure 7 demonstrated the relations between FD and the acoustic polar angle when the frequency of the sound wave and the polar angle of the incident light were fixed. In Fig. 7, we can see that FDs calculated from Δk_1 and Δk_2 decrease with the increase of acoustic polar angle, from about 3 to 12 degrees of acoustic polar angle the difference between FDs calculated from Δk_1 and Δk_2 is obvious and reach the maxima at around 6 degrees, the acoustic polar angle was usually selected in the range of 3 to 12 degrees in the design of an AOTF, so it is very important to determine the accurate calculation of momentum mismatching. Then, two AOTFs designed with acoustic polar angles of 9.52 and 6.64 degrees were selected for the FDs measurement and the experimental results exhibited a good agreement with the theoretical calculations with Δk_2 . Combining this observation with the theoretical curves shown in Fig. 3, it could be concluded that the acoustic energy shift caused by strong AO anisotropy did not affect or alter the momentum matching condition of the AO effect. The frequency corresponding to the momentum matching remained constant. However, it significantly influenced aspects such as the aperture size and magnitude of the transfer function, as well as the rate of variation with ultrasound frequency (in the form of momentum mismatching). In conclusion, the comparison between experimental and theoretical results demonstrated that the deviation of acoustic energy induced by strong AO anisotropy in crystals could not be simply overlooked. Therefore, comprehensive consideration

of this factor was imperative in the accurate design of AOTF which will have better performance in the field including optical sensing, machine learning and etc. [24,25].

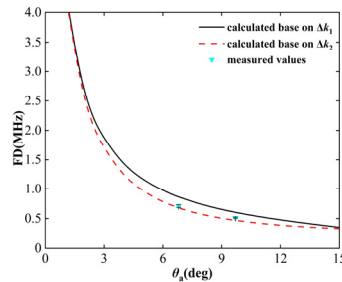


Fig. 7. Calculated and measured relationship between FD and θ_a

4. Conclusion

In this study, theoretical calculations of momentum mismatching in AO interaction were conducted with and without considering the acoustic anisotropy of the crystal. The experimental results were in agreement with the theoretical expectation considering the acoustic energy shift. The results demonstrated that the acoustic energy shift should be considered in the accurate design of AOTF.

Funding. Natural Science Foundation of Fujian Province (2020J01153, 2022J01627).

Disclosures. The authors declare no conflicts of interest.

Data availability. Data underlying the results presented in this paper are not publicly available at this time but may be obtained from the authors upon reasonable request.

References

1. K. B. Yushkov, V. Y. Molchanov, P. V. Belousov, *et al.*, "Contrast enhancement in microscopy of human thyroid tumors by means of acousto-optic adaptive spatial filtering," *J. Biomed. Opt.* **21**(1), 016003 (2016).
2. A. Machikhin, V. Batshev, V. Pozhar, *et al.*, "Acousto-optic tunable spectral filtration of stereoscopic images," *Opt. Lett.* **43**(5), 1087–1090 (2018).
3. Y. Chu, L. Chen, H. Wang, *et al.*, "Research on edge enhancement of optical image based on acousto-optic filtering," *Proc. SPIE* **12057**, 1084–1088 (2021).
4. K. B. Yushkov, M. I. Kupreychik, D. V. Obydenov, *et al.*, "Acousto-optic k-space filtering for multifrequency laser beam shaping," *J. Opt.* **25**(1), 014002 (2023).
5. C. Samuel, T. Vi Khanh, W. Vivien, *et al.*, "Interaction of giant unilamellar vesicles with the surface nanostructures on dragonfly wings," *Langmuir* **35**(6), 2422–2430 (2019).
6. M. Duocastella, S. Surdo, A. Zunino, *et al.*, "Acousto-optic systems for advanced microscopy," *J. Phys. Photonics* **3**(1), 012004 (2021).
7. Z. He, C. Li, R. Xu, *et al.*, "Spectrometers based on acousto-optic tunable filters for in-situ lunar surface measurement," *J. Appl. Remote. Sens.* **13**(2), 027502 (2019).
8. A. Machikhin, V. Batshev, V. Pozhar, *et al.*, "Single-volume dual-channel acousto-optical tunable filter," *Opt. Express* **28**(2), 1150–1157 (2020).
9. J. Li, Y. Gui, R. Xu, *et al.*, "Applications of AOTF spectrometers in in situ lunar measurements," *Materials* **14**(13), 3454 (2021).
10. I. C. Chang, "Acousto-optic devices and applications," in *Handbook of optics*, Michael Bass, eds. (McGraw-Hill:New York, 1995).
11. X. Kaikai, C. Yanxu, A. Timothy, *et al.*, "Micro optical sensors based on avalanching silicon light-emitting devices monolithically integrated on chips," *Opt. Mater. Express* **9**(10), 3985 (2019).
12. J. Xu and R. Stroud, *Acousto-optic devices: principles, design, and applications* (Wiley, 1992), Chap. 2.
13. I. C. Chang, "Analysis of the noncollinear acousto-optic filter," *Electron. Lett.* **11**(25-26), 617 (1975).
14. I. C. Chang, "Tunable acousto-optic filters: an overview," *Opt. Eng.* **16**(5), 455–460 (1977).
15. V. Voloshinov and O. Mironov, "Wide-angular acousto-optical filter for the middle-infrared regime of spectrum," *Sov. Opt. Spectrosc.* **68**, 452–457 (1990).

16. V. B. Voloshinov, V. Y. Molchanov, and J. C. Mosquera, "Spectral and polarization analysis of optical images by means of acousto-optics," *Opt. Laser Technol.* **28**(2), 119–127 (1996).
17. J. C. Kastelik, M. G. Gazalet, C. Bruneel, *et al.*, "Acoustic shear wave propagation in paratellurite with reduced spreading," *J. Appl. Phys.* **74**(4), 2813–2817 (1993).
18. J. C. Kastelik, M. Gharbi, and M. G. Gazalet, "Paratellurite: propagation of the slow shear wave in the (001) plane. New formulations for the acoustic velocity and divergence," *J. Appl. Phys.* **84**(2), 671–674 (1998).
19. K. B. Yushkov, V. Y. Molchanov, V. I. Balakshy, *et al.*, "Acousto-optic transfer functions as applied to S laser beam shaping," *Proc. SPIE* **10744**, 131–144 (2018).
20. V. I. Balakshy and V. B. Voloshinov, "Acousto-optic image processing in coherent light," *Quantum Electron.* **35**(1), 85–90 (2005).
21. V. I. Balakshy, V. B. Voloshinov, T. M. Babkina, *et al.*, "Optical image processing by means of acousto-optic spatial filtration," *J. Mod. Opt.* **52**(1), 1–20 (2005).
22. M. B. Tatiana and B. V. Vitaly, "A new method of acousto-optic image processing and edge enhancement," *J. Opt. A: Pure Appl. Opt.* **3**(4), S54–S61 (2001).
23. X. Kaikai, "Silicon electro-optic micro-modulator fabricated in standard CMOS technology as components for all silicon monolithic integrated optoelectronic systems," *J. Micromech. Microeng.* **31**(5), 054001 (2021).
24. G. Arnaldo, C. Vinfcus, D. Camilo, *et al.*, "A machine learning approach for simultaneous measurement of magnetic field position and intensity with fiber Bragg grating and magnetorheological fluid," *Opt. Fiber Technol.* **56**, 102184 (2020).
25. Z. Ji, Z. He, Y. Gui, *et al.*, "Research and application validation of a feature wavelength selection method based on acousto-optic tunable filter (AOTF) and automatic machine learning (AutoML)," *Materials* **15**(8), 2826 (2022).